Ocean Dynamics (2017) 67:783–798
DOI 10.1007/s10236-017-1059-y

Vertical mixing and elements of mesoscale dynamics over North Carolina shelf and contiguous Gulf Stream waters

Iossif Lozovatsky[1] · **Jesus Planella-Morato**[1,3] · **Kipp Shearman**[4] · **Qing Wang**[5] · **Harindra Joseph S. Fernando**[1,2]

Received: 30 September 2016 / Accepted: 24 April 2017 / Published online: 6 May 2017

Abstract Results of microstructure measurements conducted in October–November of 2015 as a part of the Coupled Air Sea Processes and Electromagnetic Ducting Research (CASPER) project are discussed. The measurements were taken on the North Carolina shelf and across the Gulf Stream front. On the shelf, the oceanic stratification was influenced by highly variable surface salinity and along-bottom advection. Vertical mixing was mostly governed by variable winds. The vertical eddy diffusivity was estimated using the VMP-based dissipation measurements, and the diffusivity values obtained during calm periods and stormy winds were compared. Parameterization of the diffusivity for various mesoscale dynamical conditions is discussed in terms of shear instabilities and internal wave-generated turbulence based on data obtained in deep waters of the Gulf Stream and on the continental slope.

This article is part of the Topical Collection on the *48th International Liège Colloquium on Ocean Dynamics, Liège, Belgium, 23–27 May 2016*

Responsible Editor: Simon Ruiz

✉ Iossif Lozovatsky
i.lozovatsky@nd.edu

[1] Department of Civil and Environmental Engineering and Earth Sciences, University of Notre Dame, Notre Dame, IN, USA

[2] Department of Aerospace and Mechanical Engineering, University of Notre Dame, Notre Dame, IN, USA

[3] Department of Physics, University of Girona, Girona, Catalonia, Spain

[4] College of Earth, Ocean, and Atmospheric Sciences, Oregon State University, Corvallis, OR, USA

[5] Naval Postgraduate School, Monterey, CA, USA

Keywords Turbulence · Mixing · Intrusions · Internal waves · Gulf Stream · North Carolina shelf

1 Introduction

Air temperature and water vapor gradients in transition zones between the land and the ocean shelf as well as between different water masses substantially affect the propagation of electromagnetic waves (EM ducting) in the marine atmospheric boundary layer (Thompson and Haack 2011; Geernaert 2007). As for the latter, an example is the sharp oceanic fronts, such as the Gulf Stream (GS) cold wall, where the rate of evaporation may greatly differ on the warm and cold sides of the front, being dependent on the wind speed, the air humidity, and the sea surface temperature (SST). The humidity and SST gradients in the atmospheric marine boundary layer affect the development of evaporative ducts, which is critical in radar operations, both communications and object detection. The SST depends not only on the atmospheric fluxes, state of the sea surface, and horizontal and vertical advections of sea water but also on turbulence and associated mixing in the water interior. The ocean surface layer can be well-mixed or stratified, and its depth is mainly determined by wind and convective mixing, lateral advection, stratification, and turbulent mixing in the underlying pycnocline. Therefore, microstructure measurements in the upper 100–200 m of the ocean or through the entire water column at shallow depths can provide valuable information on the turbulent kinetic energy (TKE) dissipation rate ε and vertical eddy diffusivity K_z (Osborn 1980) in various mesoscale (30–100 km) and submesoscale (1–10 km or less) dynamical structures (e.g., Thomas et al. 2008; Gula et al. 2016), depending on prevailing energetic processes. Comprehensive measurements shedding light on small-scale turbulence and associated frontal

dynamics (down to sub-mesoscale features) have been reported by D'Asaro et al. (2011) for Kuroshio, Thomas et al. (2016) for Gulf Stream, and Jinadasa et al. (2016) for Bay of Bengal.

The Coupled Air Sea Processes and Electromagnetic Ducting Research (CASPER) program has been developed to study EM ducting in coastal areas. The CASPER-East field campaign (http://met.nps.edu/~qwang/casper/home/home.php) was conducted on the North Carolina (NC) shelf and in contiguous waters of Gulf Stream during October–November 2015, and this paper discusses several aspects of microstructure measurements during its oceanographic component. The CASPER microstructure measurements were carried out by R/V Atlantic Explorer (Bermuda Institute of Ocean Sciences; http://www.bios.edu/ship-ops) on the shelf to the east of the coastal village Duck, NC and also in deep waters of the Gulf Stream. A bathymetric map of the region showing locations of the measurements is in Fig. 1. The analysis of microstructure data presented in this paper is focused on observations at two shelf stations R02 (75.61° W, 36.18° N) and R30 (75.14° W, 36.18° N) conducted on October 13–21, 2015 and located 2 and 30 miles away from the coast, respectively. Three blue water stations (GS_S, GS_N, and R56; October 31 and November 1, 2015) were taken at the southern and northern ends of the hydrographic transect across the Gulf Stream and at the slope, where oceanic microstructure could be influenced by various mesoscale and sub-mesoscale processes associated with the Gulf Stream. Note that sub-mesoscale structures are controlled by the Rossby number $Ro = U/Lf$ that is close to unity (e.g., McWilliams 1985, 2008). Here, U and L are characteristic velocity and length scales and f is the Coriolis parameter. For characteristic $f \approx 8.6 \times 10^{-5}$/s in the region and surface currents on the shelf $U_{shl} \sim 0.3 - 0.4$ m/s, the horizontal scales of the structures pertained to $Ro \sim O(1)$ are $L_{shl} \sim 3 - 4$ km. For much higher velocities in the Gulf Stream, $U_{gs} \sim 1 - 2$ m/s, the scales of sub-mesoscale structures may grow to 10–20 km, which could be resolved along the transect.

Note that the estimates of TKE dissipation rate for NC shelf have been reported first by St. Laurent (2009). The data were obtained in the Onslow Bay, and are compared with our shelf measurements in Sect. 3. The history of the dissipation measurements in various sections of the Gulf Stream is richer, but mostly has been carried out decades ago (Oakey and Elliott 1977; Gregg and Sanford 1980; Osborn 1980; Gargett and Osborn 1981; Lueck and Osborn 1984; Winkel et al. 2002). Newer comprehensive field campaigns that allow linking small-scale turbulence with some features of mesoscale and sub-mesoscale GS dynamics were taken in 2007 (Inoue et al. 2010) and 2012 (Thomas et al. 2016) in the regions hundreds of miles to the northeast from our GS measurements, which are described in Sect. 4. Section 5 summarizes major findings of the current study.

2 Instrumentation, data collection, and processing

The turbulence and stratification data were collected using a vertical microstructure profiler (VMP)-500 (http://rocklandscientific.com/products/profilers/vmp-500/) from the sea surfaces down to ~17 m (at R02; 38 casts total) and 30–33 m (R30; 37 casts) on the shelf and to ~130–150 m in deep waters (14 casts in 3 locations shown in Fig. 1). The VMP carries two airfoil probes to estimate small-scale shear and the dissipation rate ε, a three-component accelerometer, a pressure sensor (depth), and a Seabird temperature–conductivity unit to obtain precise temperature, salinity, and potential density profiles. Turbulence in the upper 3–5 m near the sea surface could have been contaminated by the ship movement;

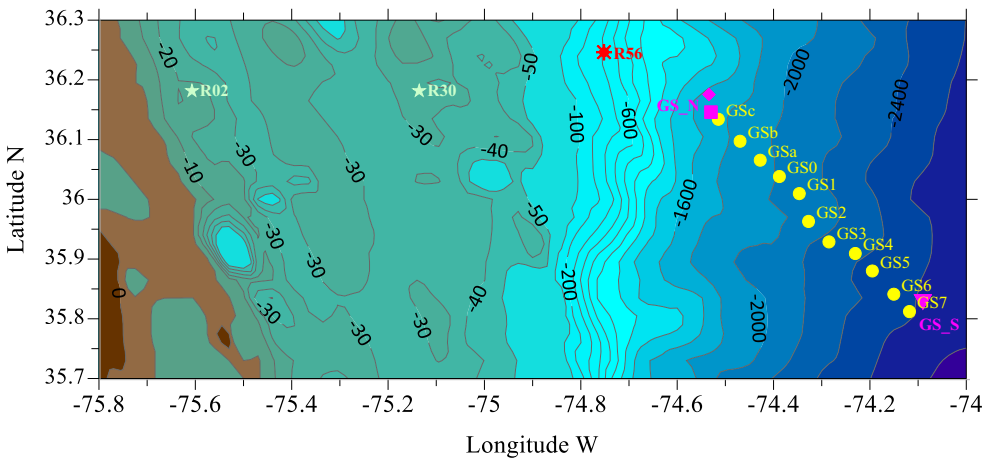

Fig. 1 The Etopo-2 bathymetry of the Casper-East measurement site with the locations of VMP stations on the North Carolina shelf (R02, φ = 36.18° N, λ = 75.61° W, ~17 m depth; R30, φ = 36.18° N, λ = 75.14° W, ~30 m depth, *stars*), near the shelf break (R56, *red snowflake*, φ = 36.25° N, λ = 74.76° W), and in the deep ocean at the southern (GS_S, φ = 35.83° N, λ = 74.1° W, *magenta triangle*) and northern (GS_N, *magenta diamond* for 10 a.m. and *square* for 8–9 p.m.; Nov 1, φ = 36.15° N, λ = 74.53° W) ends of the hydrographic transect (GSc–GS7, *yellow circles*) crossing the Gulf Stream front

thus, the dissipation rate measurements were trusted in the depth range below 5 m. The data processing of each individual cast followed the methodology of Roget et al. (2006); however, the small-scale shear spectra were fitted to Nasmyth (1970) rather than to the Panchev and Kesich (1969) canonical spectrum to calculate ε averaged over 0.5 m (on the shelf) or 1 m (deep water) segments.

During October 13–21, 2015, VMP profiling was conducted once per day in the morning around 9–10 a.m. (R30) and in the afternoon around 2–3 p.m. (R02) local time (LT). Most of the time, the ship sailed along φ = 36.18° N back and forth between these two focal stations, transmitting EM signals to another ship that sailed specific routes based on the experimental design. The ship continuously collected standard meteorological data, underway water temperature T_{w3m} and near-surface salinity S_{3m} at $z = -3$ m by the shipboard water intake system. Occasional VMP measurements were also taken between R02 and R30. The measurement cycle at R02 and R30 contained a number of consecutive VMP casts (mostly five casts in each series) to obtain the burst-averaged profiles of temperature $T(z)$, salinity $S(z)$, specific potential density $\sigma_\theta(z)$, and the TKE dissipation rate $\varepsilon(z)$ during ~15–30 min interval (the exact number of VMP casts are shown in Fig. 4b). The averaging reduced the short-term fluctuations of stratification and turbulence at various depths (the vertical coordinate z is positive upwards). The estimates of vertical eddy diffusivity used the expression $K_z \equiv K_N \sim \gamma\varepsilon/N^2$, where $N^2(z) = -(g/\rho_0) \times (d\rho_\theta/dz)$ is the squared buoyancy frequency, γ a mixing efficiency, and g, ρ_θ, and ρ_0 are the gravity, potential, and reference densities, respectively. A canonical value of $\gamma = 0.2$ was used for fully developed turbulence, although it is possible that it depends on a variety of background parameters (e.g., Lozovatsky and Fernando 2013).

The R/V Atlantic Explorer was equipped with a 75-kHz Acoustic Doppler Current Profiler (ADCP). Owing to its low vertical resolution (16 m), it was not possible to infer useful estimates of the mean vertical shear $Sh = \left[(\Delta\bar{u}/\Delta z)^2 + (\Delta\bar{v}/\Delta z)^2\right]^{1/2}$ and the gradient Richardson numbers $Ri = N^2/Sh^2$ at shallow stations R02 and R30. Here, $\bar{u}$ and $\bar{v}$ are the zonal and meridional components of mean currents. In blue water, however, the ADCP currents and vertical shear were calculated using CODAS (http://currents.soest.hawaii.edu/docs/adcp_doc/codas_doc/) software and then interpolated to a 10 m grid; the $Sh(z)$ and $Ri(z)$ profiles started at $z = -36$ m, which is the mid-point of the first unbiased bin below the sea surface.

Shipboard meteorological measurements at 12 m above the sea surface were used to calculate the wind stress and friction velocity $u_*(t)$ adjusted to a standard 10 m height. The buoyancy flux $J_b(t)$ was estimated following Shay and Gregg (1986), using the bulk-formula scripts of Matlab air–sea toolbox (http://woodshole.er.usgs.gov/operations/sea-mat/air_sea-html/index.html). It appears (Fig. 2) that during the first 3.5 days of observations, warm easterly winds (mean wind speed $W_{10} = W_a = 5.9$ m/s) prevailed over the shelf. The averaged air temperature $\overline{T}_a = 20.6^\circ$C was less than only one degree below the water temperature $\overline{T}_{w3m} = 21.45^\circ$C. At mid-day of October 16, the wind direction sharply changed toward the south, and this northerly wind dominated over the shelf until October 20. On October 18–19, the wind speed W_a increased to 12–14 m/s and the air temperature dropped to 11–12 °C. Only at the end of October 20, the cold northerly wind ceased to 2–3 m/s. Warmer easterly and southerly winds returned after this mild storm, and on October 21, the air temperature T_a rose to 17–18 °C. The water temperature $\overline{T}_{w3m}$ gradually decreased during the storm, almost catching up with T_a on October 21 (Fig. 2). The surface salinity S_{3m}, in contrast to T_{w3m}, depicts substantial spatial variations when the ship sailed along 36.18° N between R02 and R30 (see Fig. 2). The difference of salinity between relatively fresh coastal (R02) and more saline mid-shelf (R30) waters was about 4 psu on the average. On the mid-shelf, the salinity did not change much during the first 3.5 days of observations (S_{3m} ~33–33.1 psu), increasing to ~33.6–34 psu after the storm. Near the coast, however, S_{3m} was steadily increasing day by day from 28.8 to ~30 psu, but on October 18, when the northerly winds ceased, S_{3m} rapidly decreased again to 28 psu on October 20.

The observed spatial-temporal variations of salinity on the inner shelf were mostly caused by alternative advection of relatively fresh estuarine and highly saline ocean water on shelf, depending on the direction of dominant winds. Indeed, the HYbrid Coordinate Ocean Model (HYCOM; https://hycom.org/hycom) simulated surface currents (Fig. 3; the maps were adopted from http://assets.maracoos.org/) clearly show that on October 16, the freshwater outflow from Albemarle Sound was partially blocked near R02 by along shore (north-west directed) shelf currents, causing the observed increase of S_{3m} on inner shelf. On October 19, however, the opposite inflow of saline water into Albemarle Sound was driven by northerly stormy winds. On October 20–21, fresh estuarine water restored its flow out of Albemarle Sound onto the shelf (Oct 21; Fig. 3), being supported by the restored easterly winds. As a result, the near coast surface salinity rapidly reduced. On the other hand, relatively gradual increase of S_{3m} on mid-shelf near R30 was probably associated with currents entering on shelf from the shelf break to the east of R30 (Oct 19; Fig. 3).

This brief analysis of hydrometeorological conditions for the duration of our VMP measurements points to wind-driven aspects of mesoscale dynamics on the NC shelf. In addition to wind forcing and freshwater discharge in the surface layer, barotropic tidal currents and episodic intrusions of Gulf Stream water mainly in the bottom boundary layer (BBL) shaped the mesoscale background conditions for turbulence and mixing in the region. Note that the mean currents and

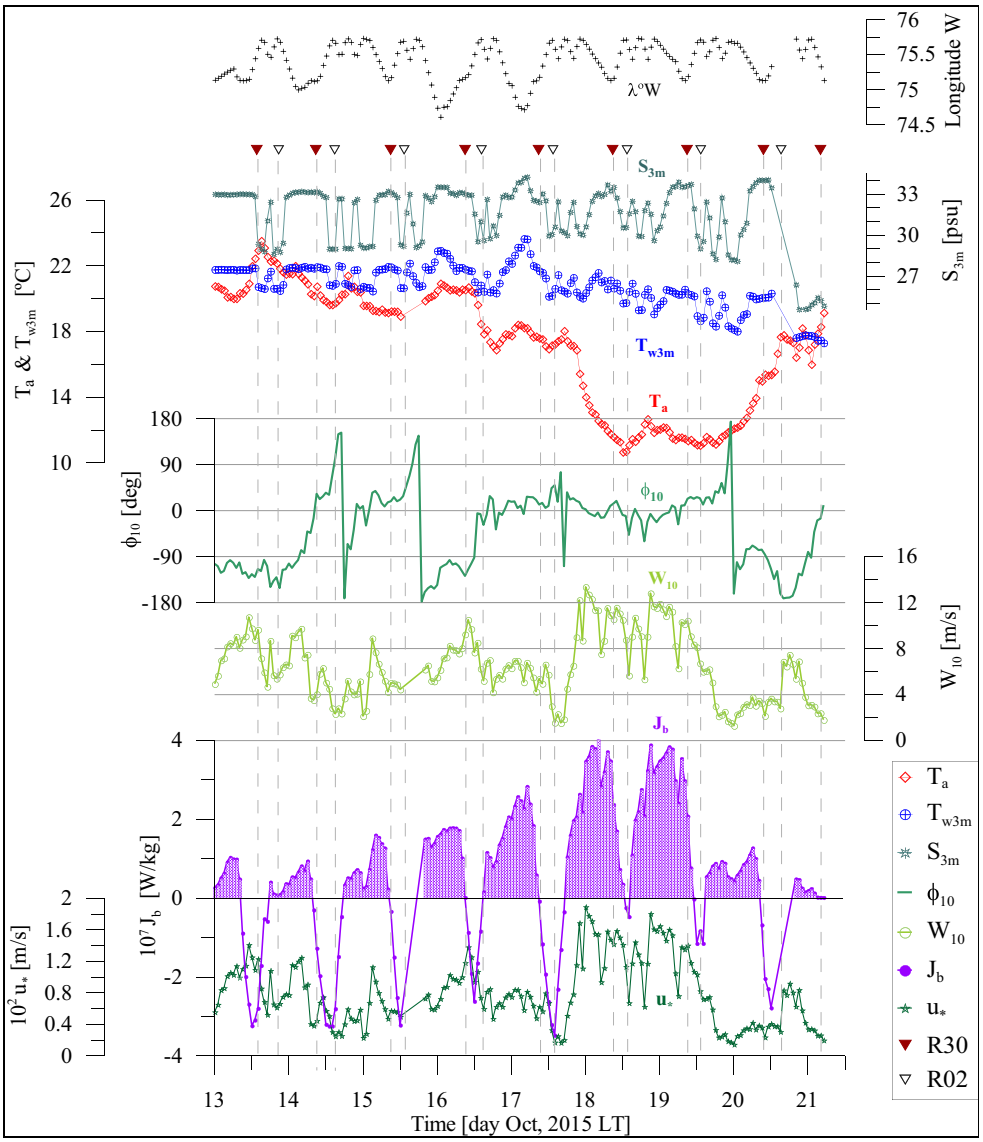

Fig. 2 The ship track between R02 (*open triangles*) and R30 (*filled triangles*) (the longitude λ along 36.18°N); the sea surface temperature T_{w3m} and salinity S_{w3m} (at $z = -3$ m); the air temperature T_a, wind direction ϕ_{10} and wind speed $W_a = W_{10}$, at 10 m above the sea surface; buoyancy J_b flux and friction velocity u_* at the sea surface (every second sample is plotted). All meteorological data are 30 min averages

stratification on the NC shelf have been thoroughly explored during Coastal Ocean Processes Inner Shelf (CoOP94) study, leading to an extensively list of publications (e.g., Lentz et al. 1999; Austin and Lentz 1999; Rennie et al. 1999; Lentz 2001; Lentz et al. 2001, to name a few).

3 Turbulence and mixing on the NC shelf

As mentioned, to our knowledge, the only prior turbulence measurements on the NC shelf have been taken on November 5–11, 2009 in Onslow Bay between ~34°–34° 25′ N and 76° 55′–76° 45′ W (St. Laurent 2009), about 100 miles to the south of the CASPER site at shallow depths of 30–35 m. The TKE dissipation rate ε therein ranged from ~10^{-9} to 10^{-6} W/kg, being influenced by the variations of stratification, from well-mixed conditions to multi-layered structures, mainly due to the variable amount of freshwater discharge to the bay. The temperature and salinity profiles reported by St. Laurent (2009) show structures similar to those obtained in our measurements, which are shown in Fig. 4a, b for R02 and R30, respectively. The most prominent thermohaline feature in the figures is the along-bottom intrusion of a warmer, saline GS water, which occupied the lower ~10 m at R30 and ~7 m at R02 between October 13 and October 18. The highest temperature 24.48 °C and salinity 34.79 psu of this intrusion occurred on October 16 at R30, and the corresponding maxima at R02 were 21.32 °C, with 32.15 psu on the same day. The intrusion was stably stratified $N^2 \sim (4-5) \times 10^{-4}$ /s^2 at R30 and $N^2 \sim (8-9) \times 10^{-5}$/s^2 at R02, indicating that bottom friction did not produce substantial turbulent mixing in the BBL. The dissipation profiles in Fig. 4a, b are consistent with this notion, showing a low level of the dissipation rate ($\varepsilon < \sim 10^{-8}$ W/kg) on the mid-shelf as well as at the shallower depths near the coast.

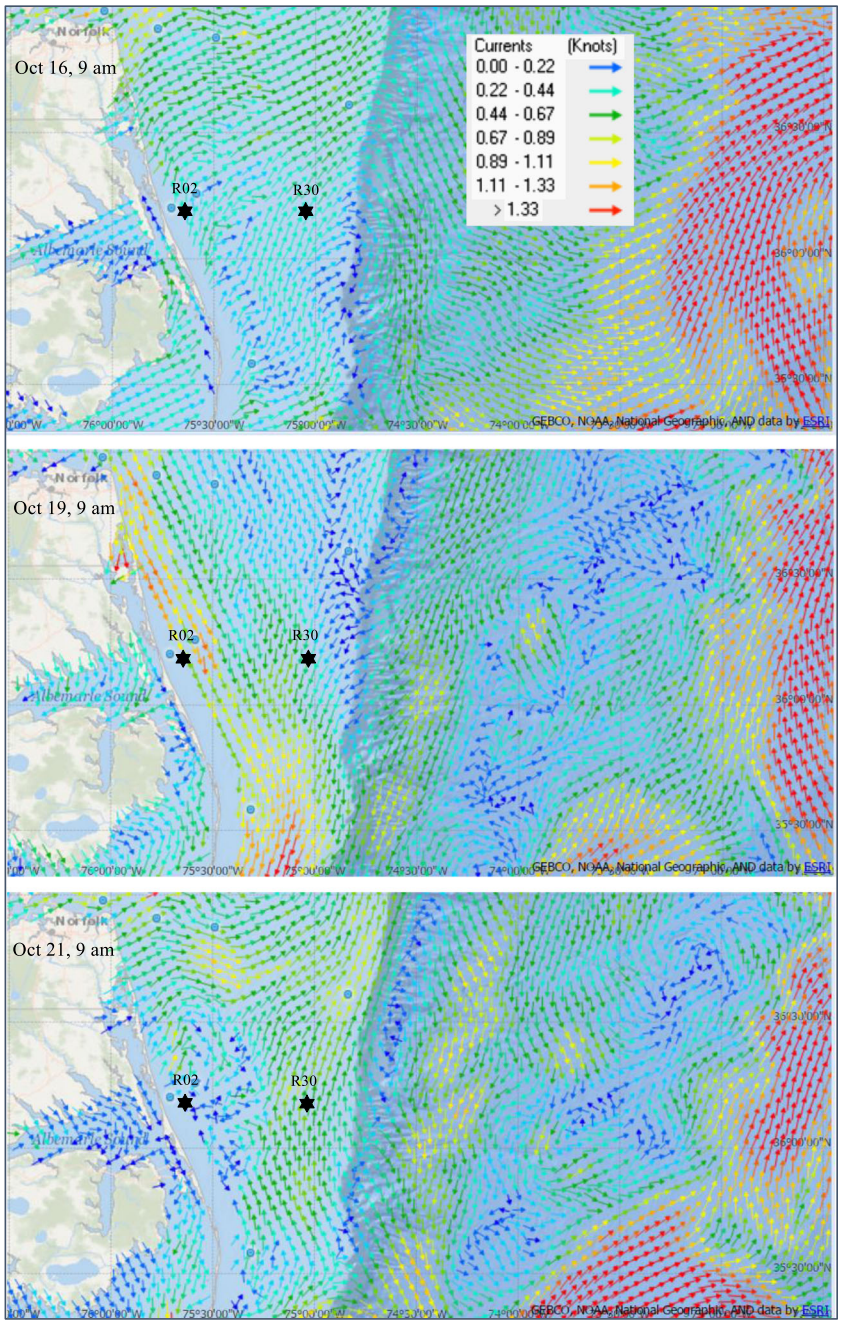

Fig. 3 The HYCOM simulated surface currents for October 16, 19, and 21, 2015 at 9 a.m. local time. The distance between R02 and R30 is about 50 km. The data are from http://assets.maracoos.org

During the storm (see wind vectors for October 18–19 in Fig. 4), the intrusion was annihilated. The water column became completely mixed closer to the coast (R02), but at R30, fragments of a weak near-bottom thermohalocline remained above the BBL because of two opposite influences of the storm. First, wind-driven horizontal advection of colder more salinity stratified water from the north (see the wind and current vectors in Fig. 4b and Fig. 3 for October 18–19) tends to strengthen stratification at R30 at all depths. Thus, the wind generated turbulence at the sea surface was forced to work against this stronger stratification, producing less effective vertical mixing. At the beginning of the storm, downward penetration of TKE was impeded by strong near-surface pycnocline (the mean buoyancy frequency $N_p \sim 4.5 \times 10^{-2}$/s) developed a day earlier due to the appearance of a lower-saline lens in the upper 10 m of the mixed layer, $h_0 = 10$ m. This effect in combination with lateral advection at all depths could explain the observed incomplete homogeneity of the water column on the mid-shelf. The mixed layer model of Pollard et al. (1972) can be used to estimate (Lozovatsky et al. 2005) the approximate final depth z_{mx} of a 10-m-deep

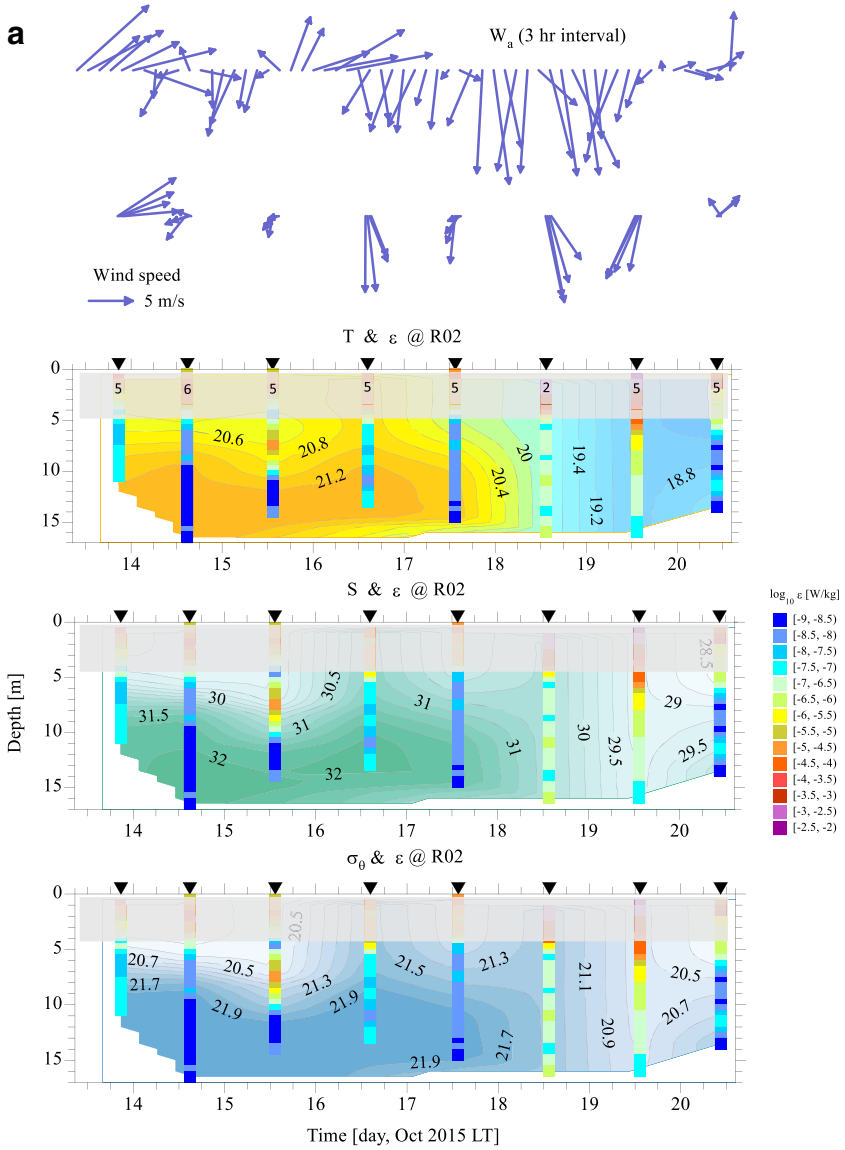

Fig. 4 **a** Temperature T, salinity S, and specific potential density σ_θ contour plots overlaid by the averaged TKE dissipation rate ε profiles at R02 (the upper 5 m are blanked as ε in this layer could be affected by ship movement). The number of VMP casts in each series is given in the upper panel below *black triangles*. The time averaged (every 3 h) wind vectors W_a (t) are on the very *top*; *below* are the wind vectors for the duration of dissipation measurements. **b** Temperature T, salinity S, and specific potential density σ_θ contour plots overlaid by the averaged TKE dissipation rate ε profiles at R30 (the upper 5 m are blanked as ε in this layer could be affected by ship movement). The number of VMP casts in each series is given in the *upper panel below black triangles*. The time averaged (every 3 h) wind vectors W_a (t) are on the very *top*; *below* are the wind vectors for the duration of dissipation measurements

mixed layer with underlying stable stratification subject to a wind stress, viz.,

$$z_{mx} = 2^{3/4}\mu_*/\sqrt{N_p f}, \quad (1)$$

where the Coriolis parameter $f = 0.86 \times 10^{-4}$/s and the mean friction velocity during October 18 $u_* = 1.3 \times 10^{-2}$ m/s (see Fig. 2). The calculated value is $z_{mx} = 11.3$ m, leading to a mixed layer depth (MLD) of $h_{mx} = h_0 + z_{mx} \approx 21 - 22$ m, which agrees reasonably well with what observed on October 19 (Fig. 4b).

The averaged dissipation rate profiles $\tilde{\varepsilon}(z)$ shown in Fig. 4b for the mid-shelf suggest that turbulence below the surface layer was generally weak under light and mild winds. On October 15, for example, the characteristic values of $\tilde{\varepsilon}(z)$ in the upper quasi-homogeneous layer (between 5 and 22 m) were in the range $(2-3) \times 10^{-9} - (1-2) \times 10^{-8}$ W/kg. However, after a mild storm on October 19, the dissipation rate in the same almost unstratified depth range increased up to $\tilde{\varepsilon} \sim (0.6\text{–}3) \times 10^{-7}$ W/kg, approximately in accordance with the boundary layer (law of the wall) scaling $\varepsilon_{lw}(z) = u_*^3/\kappa z$ for unstratified flow; here, $\kappa = 0.4$ is the Karman constant.

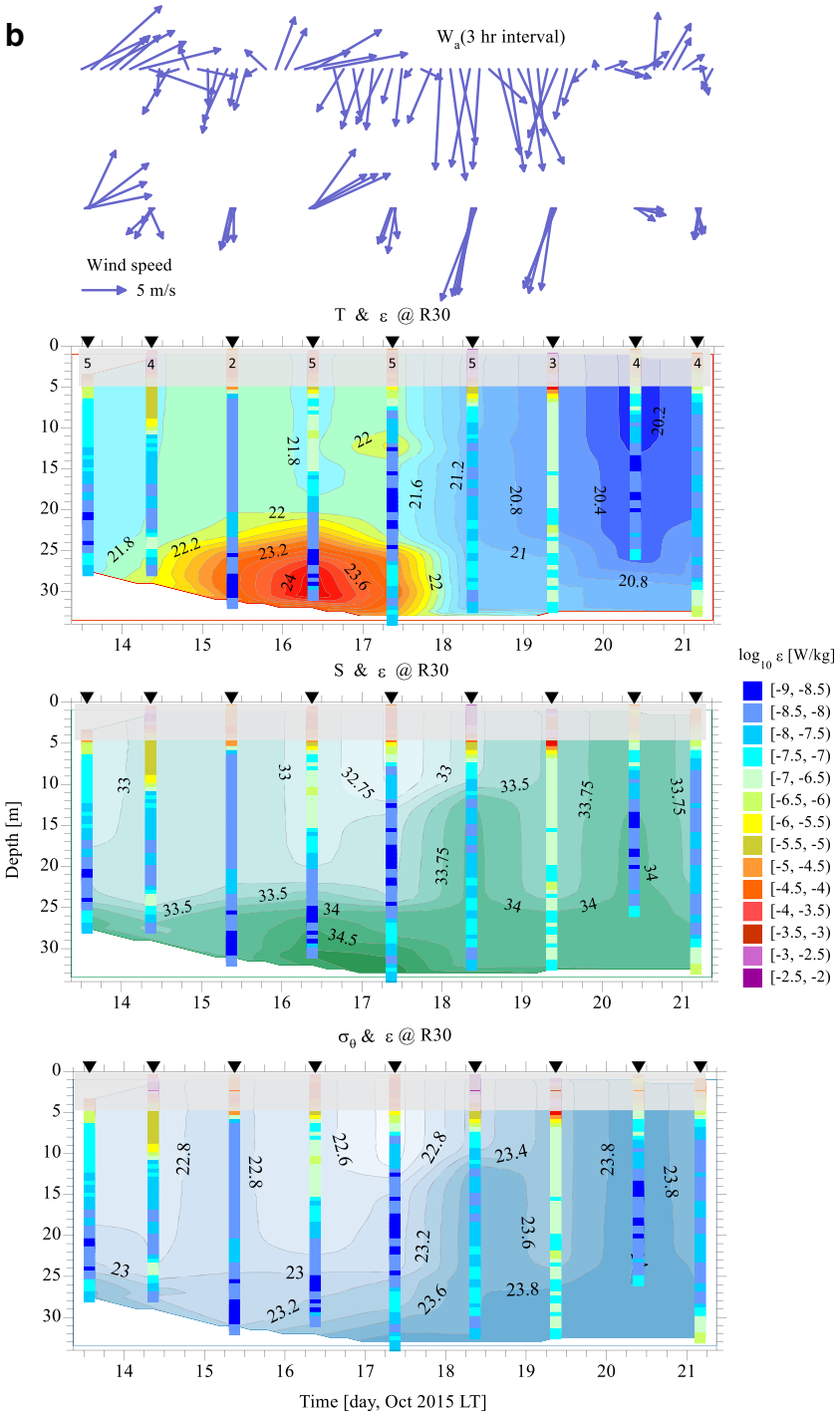

Fig. 4 (continued)

The observed $\tilde{\varepsilon}(z)$ profiles on October 15 and 19, however, were underestimated by $\varepsilon_{lw}(z)$, about 1.2 and more than two times under moderate and stormy winds, respectively. This could be explained following the work of Anis and Moum (1995); during the growing phase of wind waves (during the storm, in our case), certain amount of wind energy and momentum is consumed by the wave generation. Thus, the mixed layer turbulence $\varepsilon_{lw}(z)$ below the wind waves should be scaled by the residual fraction of the original friction velocity u_* estimated at 10 m above the sea surface.

The wind-induced turbulence, which was dominant on the NC shelf, produced vertical mixing that can be quantified by the diffusivity profiles $K_M(z)$ shown in Fig. 5a, b for R02 and R30, respectively. During non-stormy periods, the diffusivities near the coast were relatively small in the lower part of the water column ($z > -9$ m), varying from almost molecular

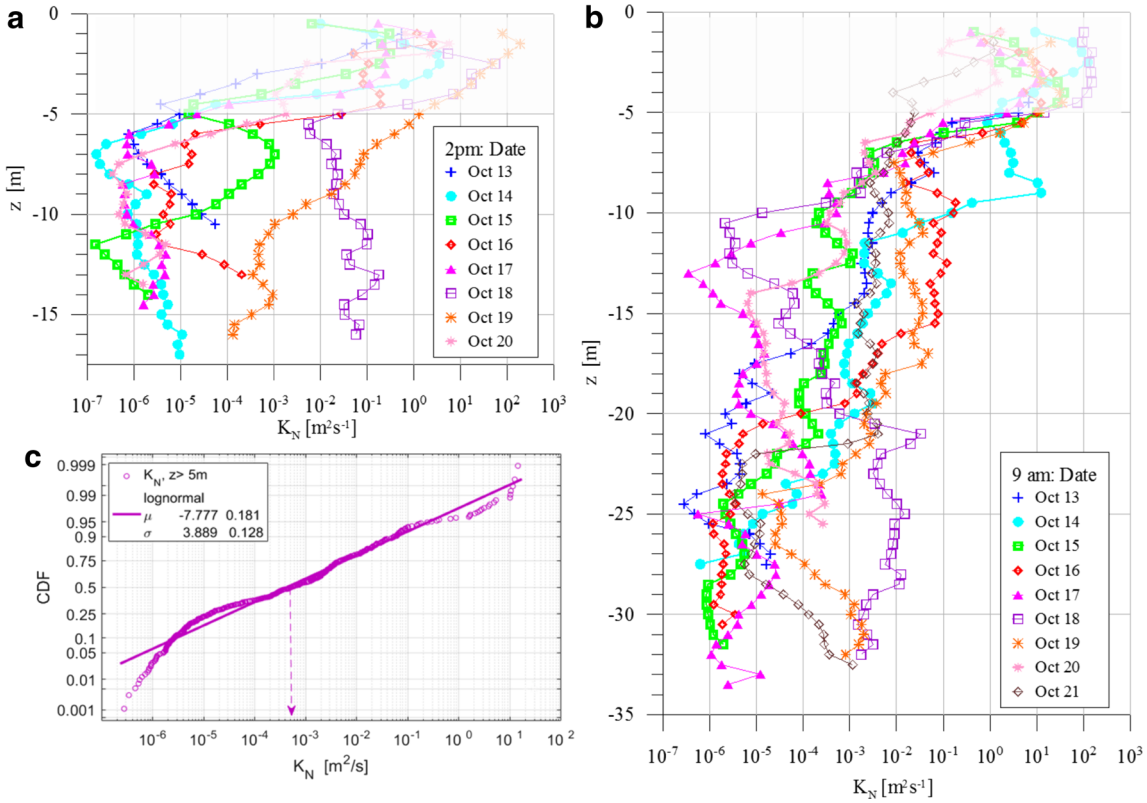

Fig. 5 The eddy diffusivity profiles $K_N(z)$ at R02 (**a**) and R30 (**b**) (the upper 5 m are blanked as this layer could be affected by ship movement). The cumulative distribution function CDF of K_N for R30 (**c**) approximated by lognormal distribution with the parameters μ and σ given in the legend. The *arrow points* to the median value $K_N \sim 5 \times 10^{-4} m^2/s$

values up to ~10^{-5} m^2/s. Under stormy winds, however, $K_N(z)$ jumped to ~10^{-1} m^2/s on October 18, decreasing during the next days to ~10^{-3} m^2/s (below $z = -10$ m). Only on October 20, the diffusivity at R02 relaxed to pre-stormy values. Such high values of diffusivity ($10^{-1} - 10^{-3} m^2/s$), nevertheless, should be viewed with caution because variable, but stable density gradient is almost completely destroyed by the storm, leading to very small and possibly uncertain estimates of the buoyancy frequency.

On the mid-shelf, the diffusivities in the water interior spanned over five decades during the observational period, from ~10^{-6} to ~10^{-1} m^2/s. To analyze this wide variability of K_N, the cumulative distribution function CDF (K_N) was calculated and roughly approximated by a lognormal distribution with parameters μ and σ given in the legend of Fig. 5c. The application of lognormal model to the probability distribution of eddy diffusivity has been shown and discussed in Roget et al. (2006). The diffusivities on mid-shelf are characterized by the median value $K_N \sim 5 \times 10^{-4}$ m^2/s, which only slightly exceeds the median estimate of lognormal approximation $e^{\mu} = 4.2 \times 10^{-4}$ m^2/s, and it is comparable with the values in other regions (e.g., Bastida et al. 2012). The most significant departure of the empirical CDF(K_N) from the lognormal fit is observed around $K_N \sim 10^{-5}$ m^2/s, which is probably due to relatively short sampling record (464 K_N samples below 5 m during 8 days) used for the CDF calculation.

4 Mixing in the Gulf Stream and on the slope near the shelf break

The majority of direct measurements of the TKE dissipation rate and temperature microstructure in waters affected by the Gulf Stream have been conducted closer to the northern edge of the current, in the region approximately bounded by 38°–40° N and 62°–69° W (e.g., Oakey and Elliott 1977; Gregg and Sanford 1980; Osborn 1980; Gargett and Osborn 1981; Lueck and Osborn 1984; Thomas et al. 2016). Inoue et al. (2010) analyzed the dissipation data obtained along a hydrographic section centered at ~66° W, which crossed the GS between 37° and 39° N. Turbulence measurements in the Florida Current, which is the most southern segment of the GS, have been discussed in Winkel et al. (2002), but no estimates of mixing intensity in the central part of GS have been reported so far.

Note that the vertical diffusivity in the GS pycnocline has been found to be relatively small, which, according to Oakey and Elliott (1977) and Winkel et al. (2002), is ~(2 − 4) ×

10^{-5}m^2/s. Slightly higher diffusivities, $K_N \sim 5 \times 10^{-5}$ m^2/s, have been reported for the GS pycnocline by Osborn (1980), Gregg and Sanford (1980), and Gargett and Osborn (1981) under moderate winds. However, strong winter winds and unstable buoyancy flux at the sea surface may induce strong mixing below the surface mixed layer with diffusivities exceeding 10^{-4} m^2/s (Inoue et al. 2010).

4.1 Stratification and currents along a Gulf Stream transect

In Figs. 6 and 7, several contour plots are shown that utilize our hydrographic data across a central section of the GS. The transect (see Fig. 1) started approximately near the GS core (station GS7, SST = 27.9 °C), crossed the GS north wall (GSNW) between GS3 (SST = 26.5 °C) and GS1 (SST = 21.6 °C), and ended close to the continental slope (the lowest SST = 19.6 °C, however, was observed slightly to the south of station GSa). Several intrusions of colder less saline shelf water were observed to the north of the GSNW. Note that the underway SST and salinity measurements across the GSNW revealed an extremely sharp and narrow local front, which was visible at the sea surface and detected by the ship's radar. The temperature and salinity differences over a distance of 100 m across the front exceeded 0.5 °C and 0.6 psu,respectively (Lozovatsky et al. 2016). A submesoscale low-salinity lens/meander occupied the upper ~50 m layer of the transect, extending to the north of the GSNW for about 15 km. Salinity in the lens core dropped below 33.5 psu, indicating shelf origin of this water.

On the contrary, the main salinity maximum ($S_{max} > 36.7$ psu) was observed in the thermocline, at $z = -120$–130 m in the GS core (Fig. 6b). The depth of this maximum outcropped toward the sea surface along the sloping isothermal/isopycnal surfaces (σ_θ contours are shown in Fig. 7), losing salinity on the way. Strong horizontal density (pressure) gradients along the GS transect must induce significant geostrophic currents directed northeastward. Figure 7c shows that near the southern end of transect a high-amplitude geostrophic component, $U_{gs} = 0.7 - 1.1$ m/s, occupied the upper 90–100 m layer, indicating the proximity to the GS core. A geostrophic flow in this region with $U_{gs} > 0.1$ m/s occupied the upper ~250 m layer. The thickness of the northeastern geostrophic current decreased to about 70–100 m near the GSCW, and it almost vanished between GSa and GSb. An indication of a weak southwestern counter current can be found near the very northern station GSc. Note the possibility of a strong peripheral branch of Gulf Stream in the vicinity of the GSCW, which is seen in the upper ~70 m layer, with high-speed geostrophic flow having $U_{gs} > 1$ m/s near the sea surface.

The geostrophic component is expected to dominate the oceanic currents in the GS region, but other dynamical phenomena such as drift currents, inertial oscillations, tides, and internal wave-induced currents can also play role in determining the variables that sway the spatial structure of turbulence and vertical mixing. To this end, the total measured ADCP current vectors at every station of the CTD transect are shown in Fig. 7. The northeastward flow to the south of GSNW (GS1) corresponds well with the direction of the GS; the amplitudes of the vectors in Fig. 7a are up to 2 m/s close to the GS core (GS4–GS7, $z = -30$–40 m). Direct current measurements show much deeper penetration of GS flow compared to U_{gs}, which was calculated using the end point of each CTD cast ($z_{end} = -300$ m) as the zero level of geostrophic velocity (which is the usual approach, but it appears to be inadequate for current work). On the other hand, spatial structure of U_{gs} in Fig. 6c and current vectors in Fig. 7a are in excellent qualitative agreement (but the vector amplitudes are about twice of U_{gs}), even depicting a very weak southward current near the northern end of the transect. The only clear difference between the currents shown in Figs. 6c and Fig.7a is the absence of a peripheral GS branch near the GSCW in the ADCP data, which can be attributed to unresolved upper 30 m layer by a 75-kHz shipboard ADCP.

The mean vertical shear in the GS pycnocline appears to be not high (see Fig. 7b), which corroborates several previous GS studies (e.g., Gregg and Sanford 1980; Gargett and Osborn 1981). As a result, the gradient Richardson numbers calculated with 10 m vertical resolution exceed not only the linear limit of 0.25 but also the non-linear critical value of 1 almost everywhere along our transect, let alone near the upper boundary of the pycnocline (the depth range ~30–80 m). Only a few patches with $Ri < 1$ were observed deeper in the pycnocline, centering at $z = -190$ m (GS3) and $z = -240$–260 m (GS5 and GS6). Thus, the *Ri*-number color section shown in Fig. 7a may indicate a low probability of shear and convective instabilities ($Ri < 1$) in the GS pycnocline. However, several white-colored *Ri* segments inside the inclined portion of the pycnocline (Fig. 7a), with $1 < Ri < 1.8$, suggest the instability of Holmboe waves that usually occurs in stratified shear layers at $Ri > 1.3$ (Strang and Fernando 2001). These waves can be a possible source of the turbulence generation therein.

Direct measurements of turbulence and the estimates of eddy diffusivity are examined next.

4.2 Mixing parameterizations

The diffusivities $\overline{K}_N = 0.2\overline{\varepsilon}/\overline{N}^2$ were calculated using the original 1-m sampled estimates of $\varepsilon(z)$ obtained during a series of VMP casts at a particular station, and then averaged over consecutive 10 m depth intervals. The calculated $\overline{N}^2(z)$ were also averaged over the same 10 m segments that corresponded to $\overline{Sh}(z)$ profiles and the gradient Richardson number $\overline{Ri} = \overline{N}^2(z) \ / \overline{Sh}(z)^2$. This approach allowed to obtain pairs of $\overline{\varepsilon}$ $-\overline{Ri}$ and $\overline{K}_N - \overline{Ri}$ for further scaling analysis.

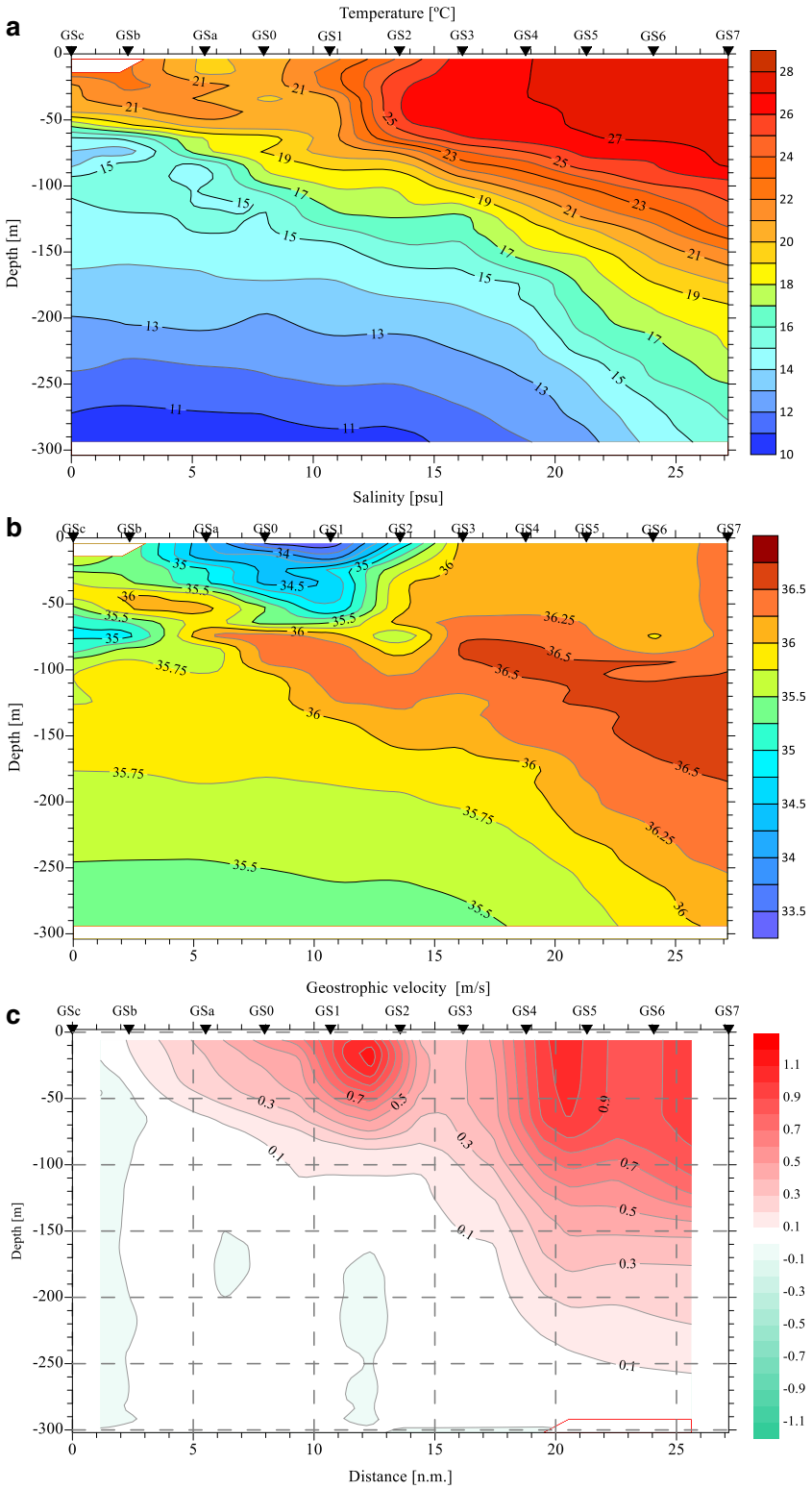

Fig. 6 The temperature (**a**), salinity (**b**), and geostrophic velocity (**c**) contour plots along the hydrographic section (Fig. 1), extending from the GS warm core (GS7) to the continental slope while crossing the GS cold wall (GS2–GS1). The distances in nautical miles start from the most northern station GSc

4.2.1 Near the Gulf Stream core

The relationship between $\overline{K}_N$ and $\overline{Ri}$ is shown in Fig. 8b for station GS_S located near the southern end of the GS transect in the vicinity of GS core, and the corresponding $T(z)$, $S(z)$, and $\sigma_\theta(z)$ profiles are presented in Fig. 8a. The $\overline{K}_N$–$\overline{Ri}$ samples shown in the regression plot are naturally partitioned into two distinct groups. The first one consists of five large blue snowflakes that are located along the best least square fit $\overline{K}_N = K_{sl}\overline{Ri}^{-1.2}$, with the coefficient of determination $r^2 = 0.97$

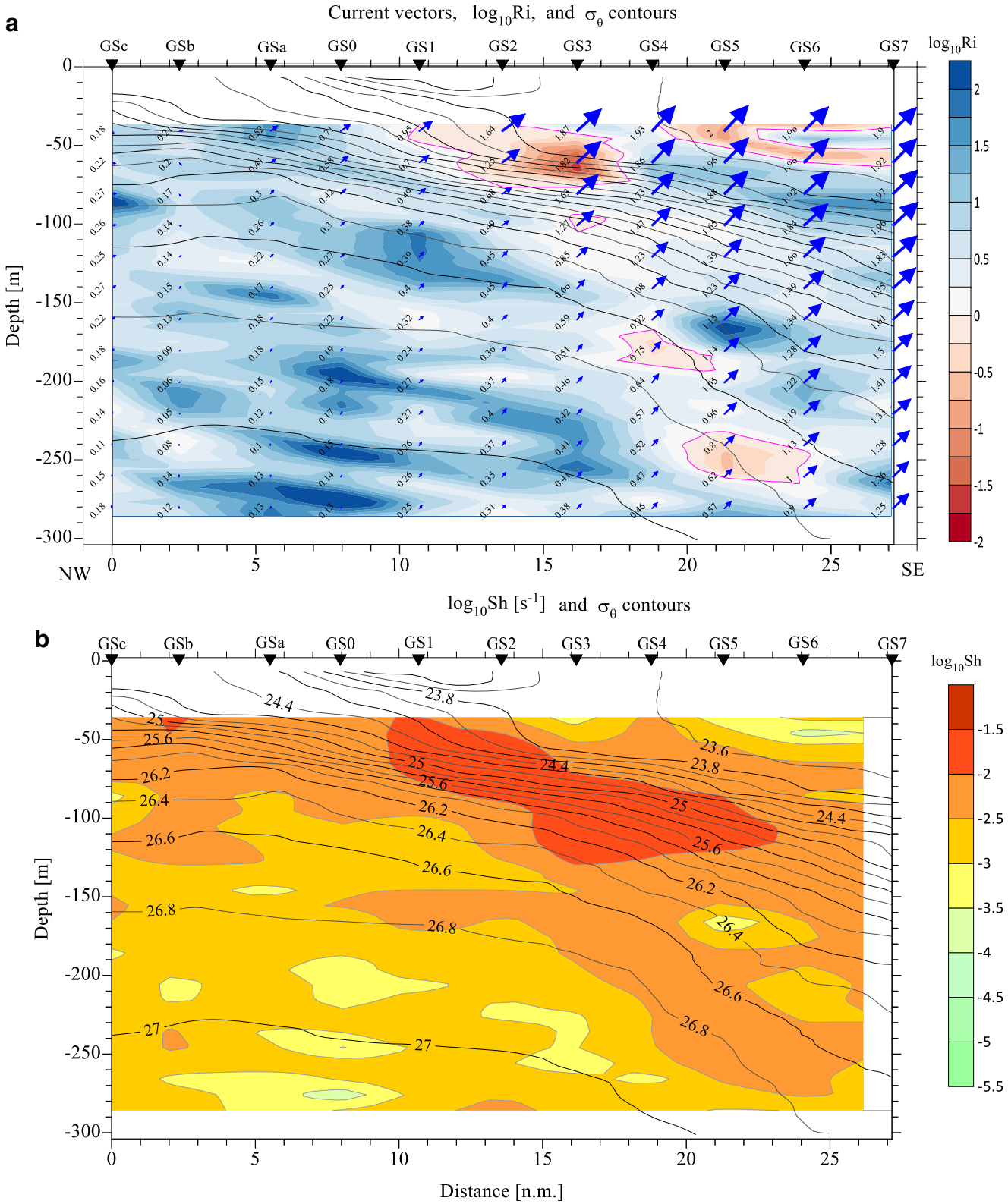

Fig. 7 The ADCP currents along the GS section over the Richardson number $\log_{10} Ri$ color palette and σ_θ contours (**a**); the vector's magnitude is proportional to the flow speed shown near the *arrows* by *numbers*. Regions with $Ri < 1$ are encircled by thin magenta lines. The vertical shear $\log_{10} Sh$ plot (**b**) is overlaid by the same σ_θ contours (labeled only here) as those shown in **a**

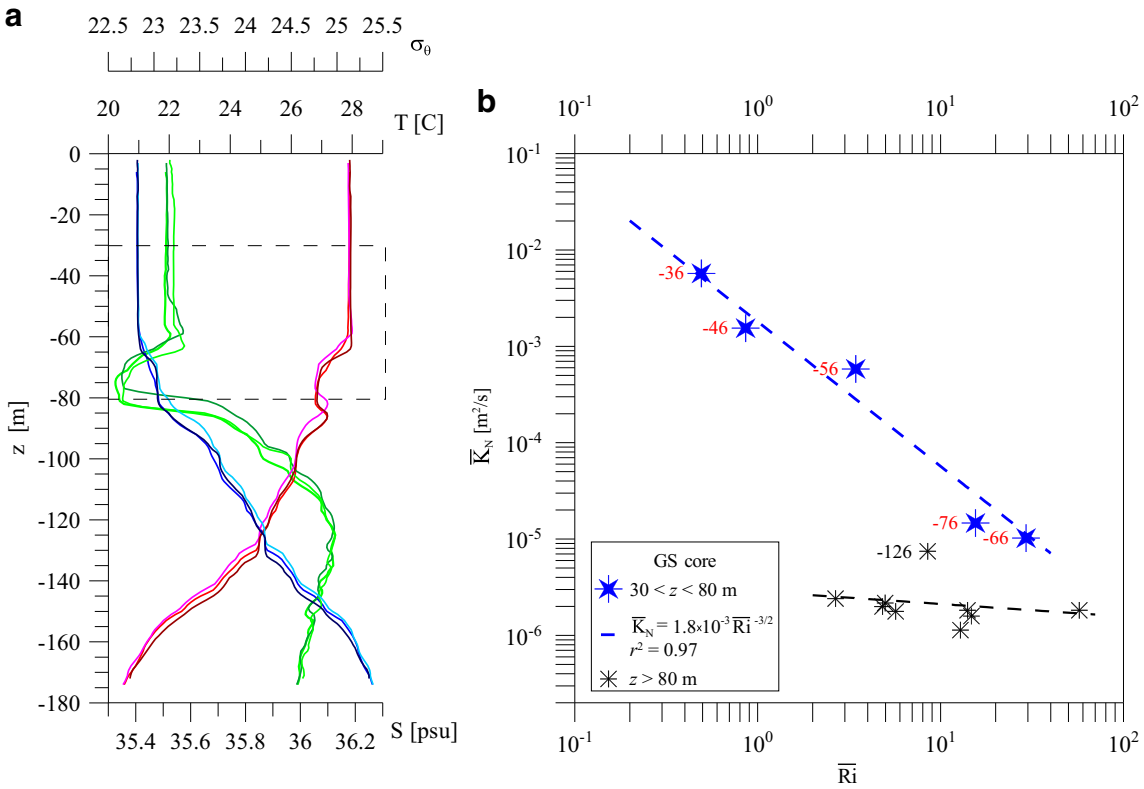

Fig. 8 *Left panel*: temperature (*red*), salinity (*green*), and specific potential density (*blue*) profiles in the GS core near GS7. *Right panel*: the diffusivity $K_N(Ri)$ as a function of the gradient Richardson number in the pycnocline ($z > -80$ m, smaller *black symbols*) and above it ($-30 < z < -80$ m, *large blue snowflakes*; the corresponding mean depths of the samples are labeled in *red*)

and the highest diffusivity recorded in the surface layer is $K_{sl} = 5.8 \times 10^{-3}$ m^2/s at $z = -36$ m. Indeed, all these samples belong to the upper turbulent, weakly stratified part of the water column. A transition layer below MLD was occupied by an intrusion of slightly less saline, colder water atop of the pycnocline. The absolute values of $\overline{K}_N$ near the core of GS flow are high, ranging between ~10^{-2} and 10^{-5} m^2/s. The rest of the diffusivity samples (smaller black snowflakes) are from the GS pycnocline, where a weak mixing at all depths is quantified by $\overline{K}_N \sim 2 \times 10^{-6}$ m^2/s with only one exception at $z = -126$ m, where $\overline{K}_N$ rises to 8.3×10^{-6} m^2/s. This indicates that a power function dependence $\overline{K}_N(\overline{Ri})$ similar to that reported in several previous studies is applicable to the surface layer of the GS core flow with shear generated turbulence (see, for example, an overview and discussion in Lozovatsky et al. 2006). On the other hand, although the mean shear is still relatively high in the GS pycnocline (Fig. 7), strong stratification therein prevents shear induced turbulence. Mixing is very weak, and the diffusivities do not depend on the gradient Richardson number.

4.2.2 Waters to the north of the GSNW

The VMP stations marked as GS_N in Fig. 1 were taken close to the northern end of the GS transect in the morning (10 a.m., diamond) and in the evening (8–9 p.m., square) of November 1. The mesoscale features in this region is much more active and variable than that near the GS core. It is affected by the GS waters and waters originated on the shelf and continental slope. A large number of narrow local frontal zones, plenty of multiple intrusions (large and small) induced by GS filaments, and meanders interacting in vertical and horizontal planes are exemplified in the GS_N VMP profiles (Fig. 10a, b). Despite the rich variety of mesoscale features to the north of GSNW, the functional dependence between $\overline{K}_N$ and $\overline{Ri}$ generally holds everywhere in the shallow pycnocline, which starts almost at the sea surface (Fig. 9a) or covered by a thin (less than 25 m) mixed layer (Fig. 9b). The main trend $\overline{K}_N \sim \overline{Ri}^{-1}$ (Fig. 9c) suggests that turbulent mixing in the layered pycnocline was mainly caused by shear generated turbulence. The two outliers in Fig. 9c at $z = -106$ and -116 m belonging to the 10 a.m. measurement Fig. 9a) may indicate a non-shear induced mixing in the lower part of a large, about 50 m thick, cold fresh intrusion, where shear near its inflection point (around $z = -106$ m, see Fig. 9a) should be negligibly small. This powerful intrusion may have had sufficient capacity to induce double-diffusive instability, generating diffusive mixing at its lower boundary under high gradient Richardson numbers (low shear). Indeed, the development of the diffusive regime of double diffusion (Turner 1973) is

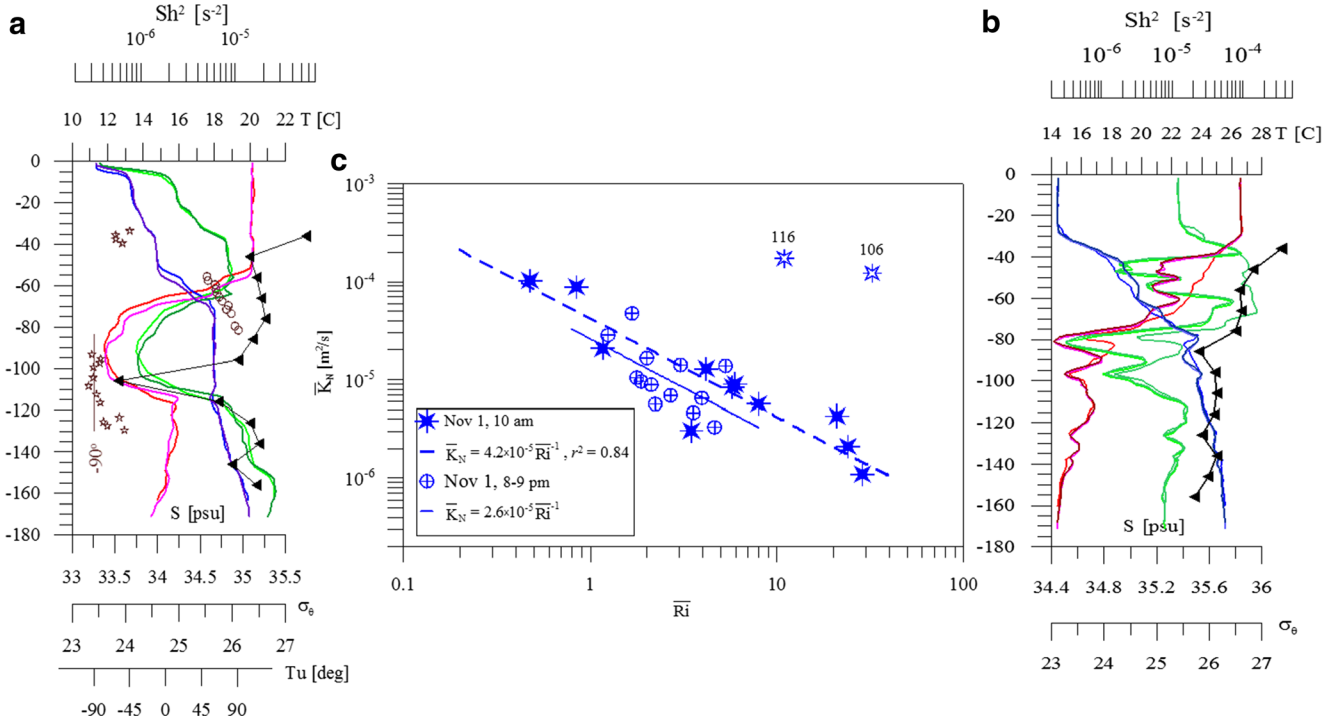

Fig. 9 Temperature (*red*), salinity (*green*), specific potential density (*blue*), and squared shear (*black triangles*) profiles at GS_N, to the north of the GSCW taken on November 1 at 10 a.m. (**a**) and 8–9 p.m. (**b**). The Turner angle (*Tu*) is in **a**: $-90^{\circ} < Tu < 45^{\circ}$ (*stars*), $-45^{\circ} < Tu < 90^{\circ}$ (*open circles*), see text for details. The eddy diffusivity—$\overline{K}_N$ —as a function of the gradient Richardson number $\overline{Ri}$ is in **c**. The depths of two outliers ($-z = 116$ and 126 m) are close to the velocity inflection point of a large cold intrusion (**a**), in which the vertical shear is very low but the possibility of diffusive convection is high ($Tu \approx -90^{\circ}$)

most probable in the depth range between ~95 and ~120 m, a claim supported by the values of Turner angle (Ruddick 1983), which are close to −90° (stars in Fig. 9a). The Turner angle is related to the stability ratio $R_\rho = -\tan(Tu + 45^{o})$, where $R_\rho = \alpha\partial_z T/\beta\partial_z S$, α and β are temperature expansion and salinity contraction coefficients, and $\partial_z T$ and $\partial_z S$ are vertical gradient of temperature and salinity, respectively. Note that double diffusive convection can also be developed in the upper part of this large intrusion where $45^{o} < Tu < 90^{o}$ (salt fingers regime, circles in Fig. 9a), but with a lower probability than the occurrence of diffusive regime below the intrusion. This is because *Tu* angles close to 90° occupy only a narrow depth range around $z = -85$ m, and importantly, there is a relatively high vertical shear at this depth that would overshadow molecular phenomena of double-diffusion.

The general outcome of above analysis is that mixing in the GS waters is mainly caused by regular shear instability, which generates turbulence almost everywhere in the pycnocline at the north frontal edge of the GS, but in the core of the GS current, mixing is only effective in a weakly stratified surface layer.

4.2.3 Continental slope near the shelf break

A special VMP station R56 (Fig. 1) was setup in deep waters on the continental slope near the NC shelf break. The measurements were taken on November 1 between the morning and the evening VMP casts at GS_N. The stratification at R56 was quite striking, exhibiting a strong narrow (~10–15 m deep) near-surface pycnocline (Fig. 10a) originated due to a low saline, cold shelf water surface lens. A stably stratified layer ($N^2_{up} \sim 1.2 \times 10^{-4}/\mathrm{s}^2$) with decreasing downward temperature and increasing salinity occupied the depth range between ~15–20 and ~55–60 m. A narrow density interface separated this upper stratified layer form a deeper, somewhat less stratified pycnocline with $N^2_{lp} \approx (4\text{–}5) \times 10^{-5}/\mathrm{s}^2$. A regression plot $\overline{K}_N\left(\overline{Ri}\right)$ shown in Fig.10b depicts a power fit (with $r^2 > 0.99$) to three samples from the upper layer, $\overline{K}_N = 1.82 \times 10^{-6}\overline{Ri}^{-0.89}$ ($Ri < 1$), suggesting continuous decrease of the diffusivity with depth. However, further down, below $z = -60$ m, the diffusivities increased several times compared to $\overline{K}_N$ ($z = -56$ m), forming a cloud of samples around $\overline{K}_N \approx 10^{-5}$ m^2/s without any particular dependence on $\overline{Ri}$. Thus, regular shear instability of the mean currents appears to play a minor role for mixing in the lower pycnocline.

To this end, we explored the influence of internal waves (IWs) on turbulence generation at the continental slope. This mechanism is especially plausible at R56, which is near the shelf break where barotropic tide often generates tidal internal waves and packets of higher frequency non-linear waves, which finally degenerate into small-scale turbulence (e.g., St.

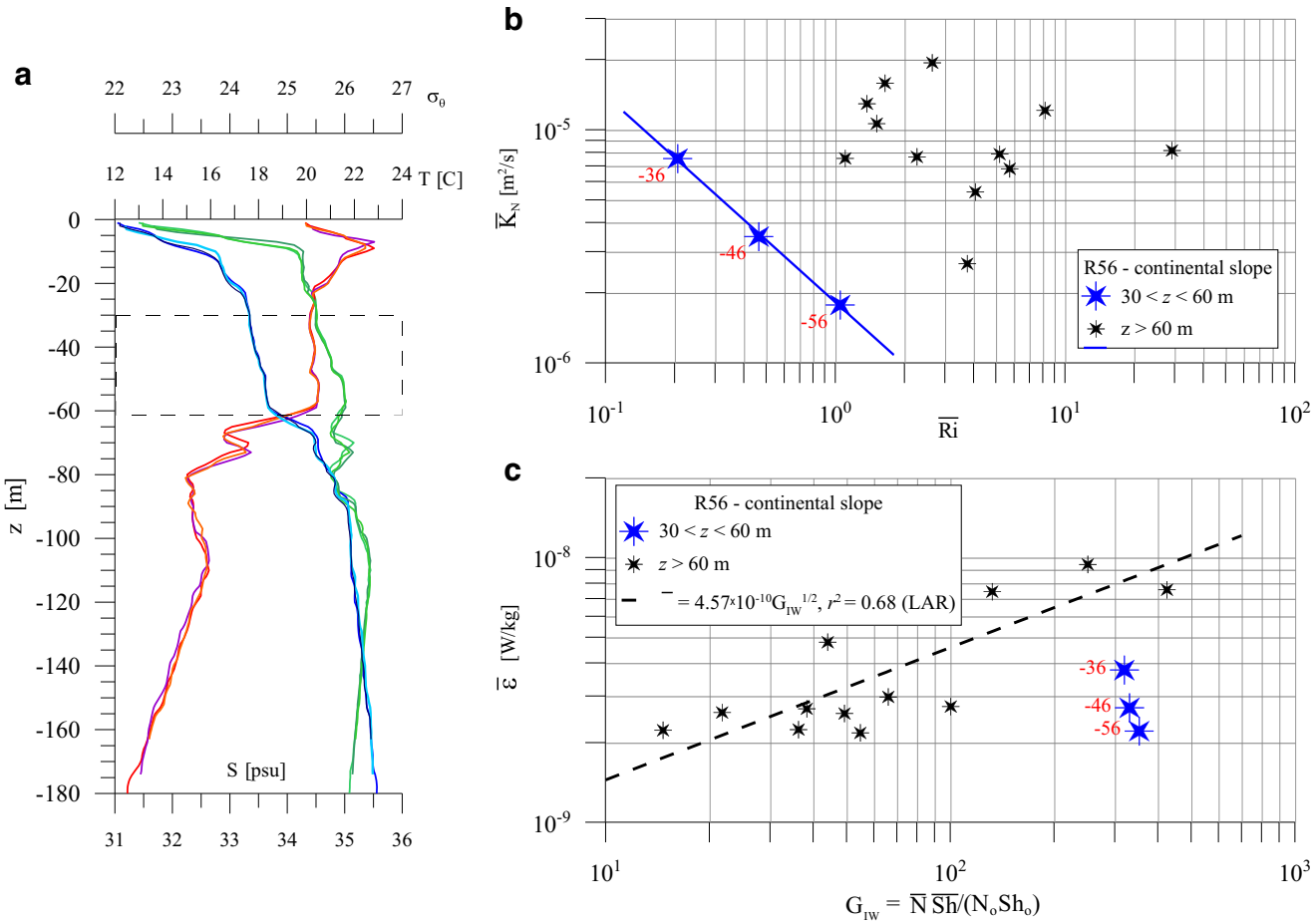

Fig. 10 Temperature (*red*), salinity (*green*), and specific potential density (*blue*) profiles on the continental slope near the NC shelf break at R56 (**a**). The diffusivity $\bar{K}_N(\bar{R}i)$ as a function of the gradient Richardson number (**b**) and the TKE dissipation rate $\bar{\varepsilon}$ as a function of the IW-turbulence parameter G_{iw} (**c**); the *large blue snowflakes* are juxtaposed by the mean depths of samples (numbers in *red*)

Laurent et al. 2011). We explored the IW-based parameterization of turbulence (MacKinnon and Gregg (2003) with respect to our data. It links the TKE dissipation rate $\overline{\varepsilon}$, not the oft-used diffusivity $\overline{K_N}$, but with the so-called IW-dissipation parameter $G_{iw} = \overline{\varepsilon}_0 \overline{NSh}/N_0 Sh_0$, where the reference values are $N_0 = Sh_0 = 3$ cph. The background dissipation $\overline{\varepsilon}_0 = 6.9 \times 10^{-10}$ W/kg was derived by Henyey et al. (1986) from an analytical model. In later studies, alternative values of N_0, Sh_0, and $\overline{\varepsilon}_0$ have been used as adjustable parameters.

The dependence between $\overline{\varepsilon}$ and G_{iw} is shown in Fig. 10c. It appears that G_{iw} in the upper pycnocline ($-36 < z < -56$ m) does not change much, and therefore, the dissipation rate $\overline{\varepsilon}$ in this depth range (large snowflakes) is almost independent of G_{iw}. All other $\overline{\varepsilon}$ samples depict growing trend of $\overline{\varepsilon}$ with increasing G_{iw}. The least square fit to these data, $\overline{\varepsilon} = \overline{\varepsilon}_0 G_{iw}^{1/2}$ with $\overline{\varepsilon}_0 = 4.57 \times 10^{-10}$ W/kg, is markedly weaker than the linear dependence suggested by MacKinnon and Gregg (2003), but it still indicates a substantial impact of internal waves on stratified turbulence in blue water on the continental slope to the north of the Gulf Stream front. The diffusivity $\overline{K_N}$, however, is only indirectly (via $\overline{\varepsilon}$) affected by G_{iw}. No specific functional dependence could be found between these two variables.

5 Conclusions

During October–November 2015, microstructure measurements were collected by R/V Atlantic Explorer on a shallow North Carolina shelf as well as in deep waters on the continental slope near the Gulf Stream northern wall and in the Gulf Stream core.

On the shelf, stratification was influenced by highly variable surface salinity, 28–31 psu near the coast and 31–34 psu on mid-shelf. The observed spatial–temporal variations of salinity on the inner shelf were caused by the advection of relatively fresh estuarine and highly saline ocean water, which was governed by the direction of dominant winds. The wind-driven dynamics on the NC shelf was the major source of small-scale turbulence and mixing in the water interior. In

addition to wind forcing and freshwater discharge to the surface layer, barotropic tidal currents and episodic intrusions of Gulf Stream water, mainly in the bottom boundary layer, shaped the mesoscale background conditions for turbulence and mixing in the region.

The daytime wind-induced turbulence on the shelf can be scaled using the law of the wall parameterization, which is satisfied in the mixed layer below the wind waves. During the growing stage of surface waves, however, the modeled dissipation rate was found to be overestimated by the bulk-formula-based friction velocity u_*. At depths below ~5 m, the dissipation rate ε was generally low, not exceeding ~2×10^{-8} W/kg. Only after a day-long stormy winds (with hourly averaged wind ~14 m/s), the water column on mid-shelf (~33 m depth) became turbulent with a characteristic dissipation rate $\varepsilon \sim 10^{-7}$ W/kg.

The vertical diffusivities K_z near the coast were relatively small in the lower half of the water column, ranging from almost molecular values up to $\sim 10^{-5}$ m^2/s during non-stormy periods. Under stormy winds, K_z jumped to $\sim 10^{-3} - 10^{-1}$ m^2/s at all depths. On mid-shelf, the diffusivities in the water interior vary over five decades with a median value of $\sim 5 \times 10^{-4}$ m^2/s.

The mean vertical shear in the Gulf Stream pycnocline was found to be fairly weak, consistent with data reported in previous studies. The gradient Richardson numbers calculated with 10 m vertical resolution exceeded the canonical critical values almost everywhere in the Gulf Stream pycnocline. Only a few patches with $Ri < 1$ were observed near the upper boundary of the pycnocline; however, in the upper mixed layer in the vicinity of the Gulf Stream core, the gradient Richardson number was sub-critical, favoring shear-induced turbulence. For shear induced turbulence, the diffusivity in GS waters shows a power dependence on Ri, $K_z \sim Ri^{-p}$, with p varying around unity.

The stratified turbulence on the slope, presumably generated by instabilities of high-frequency internal waves, showed an increase of ε in the pycnocline with increasing internal wave dissipation parameter $G_{iw} = \overline{\varepsilon}_0 \overline{NSh} / N_0 Sh_0$. The empirical relationship so obtained, $\overline{\varepsilon} = \overline{\varepsilon}_0 G_{iw}^{1/2}$ with $\overline{\varepsilon}_0 = 4.57 \times 10^{-10}$ W/kg, however, had a much weaker dependence between $\overline{\varepsilon}$ and G_{iw} than that originally suggested by MacKinnon and Gregg (2003).

More extensive data sets and theoretical studies are needed to analyze the interplay between mesoscale, sub-mesoscale, and small-scale (turbulence) dynamics more thoroughly. As reiterated by the referees, sub-meso and small-scale structures are variable in time and intermittent in space, which require substantial efforts to observe wide scales of processes simultaneously. Recent large oceanographic projects such as LATMEX (Shcherbina et al. 2015, Gulf Stream) and ASIRI (Wijesekera et al. 2016, Bay of Bengal) as well as preceding measurements in one of the Kuroshio local fronts (D'Asaro et al. 2011) are some antecedent comprehensive studies on the interdependence of sub-mesoscale dynamics and turbulence in the regions with high mesoscale activity.

Acknowledgements We are thankful to the crew of R/V Atlantic Explorer for the everyday help and care during the cruise. Our colleagues onboard of the ship Orson Hyde, Alejandra Sanchez-Rios, Ed Creegan, Adam Christman, and David Grober provided valuable assistance during the measurement program. The project was funded by the US Office of Naval Research, MURI–CASPER (NPS—N00244-14-2-0004; ONR Award N00014-17-1-3195).

References

Anis A, Moum JN (1995) Surface wave-turbulence interactions: scaling epsilon near the sea surface. J Phys Oceanogr 25:2025–2045

Austin JA, Lentz SJ (1999) The relationship between synoptic weather systems and meteorological forcing on the North Carolina inner shelf. J Geophys Res 104(C8):159–118

Bastida I, Planella J, Roget E, Guillén J, Puig P, Sánchez X (2012) Mixing dynamics on the inner shelf of the Ebro Delta. Sci Mar 76S1:31–43. doi:10.3989/scimar.03605.18A

D'Asaro E, Lee C, Rainville L, Thomas L, Harcourt R (2011) Enhanced turbulence and energy dissipation at ocean fronts. Science 332(6027):318–322. doi:10.1126/science.1201515

Gargett AE, Osborn TR (1981) Small-scale shear measurements during the Fine and Microstructure Experiment (FAME). J Geophys Res 86:1929–1944

Geernaert GL (2007) On the evaporation duct for inhomogeneous conditions in coastal regions. J Appl Meteorol and Climatol 46:538–543

Gregg M, Sanford TB (1980) Signatures of mixing from Bermuda slope, the Sargasso Sea and the Gulf Stream. J Phys Oceanogr 10:105–127

Gula J, Molemaker MJ, James C, Mc Williams JC (2016) Submesoscale dynamics of a Gulf Stream frontal eddy in the South Atlantic Bight. J Phys Oceanog 45:690–715

Henyey FS, Wright J, Flatte SM (1986) Energy and action flow through the internal wave field. J Geophys Res 91:8487–8495

Inoue R, Gregg MC, Harcourt RR (2010) Mixing rates across the Gulf Stream, part 1: on the formation of Eighteen Degree Water. J Mar Res 68:643–671

Jinadasa SUP, Lozovatsky I, Planella-Morató J, Nash JD, Mac Kinnon JA, Lucas AJ, Wijesekera HW, Fernando HJS (2016) Ocean turbulence and mixing around Sri Lanka and in adjacent waters of the northern bay of Bengal. Oceanography 29(2):170–179

Lentz S, Guza RT, Elgar S, Feddersen F, Herbers THC (1999) Momentum balances on the North Carolina inner shelf. J Geophys Res 104(C8):18, 205–18, 226

Lentz SJ (2001) The influence of stratification on the wind-driven cross-shelf circulation over the North Carolina shelf. J Phys Oceanogr 31(9):2749–2760

Lentz S, Carr M, Herbers THC (2001) Barotropic tides on the North Carolina shelf. J Phys Oceanogr 31(7):1843–1859

Lozovatsky I, Figueroa M, Roget E, Fernando HJS, Shapovalov S (2005) Observations and scaling of the upper mixed layer in the North Atlantic. J Geophys Res 110:C05013. doi:10.1029/2004JC002708

Lozovatsky I, Roget E, Fernando HJS, Figueroa M, Shapovalov S (2006) Sheared turbulence in a weakly-stratified upper ocean. Deep-Sea Res I 53:387–407. doi:10.1016/j.dsr. 2005.10.002

Lozovatsky I, Fernando HJS (2013) Mixing efficiency in natural flows. Phil Trans Roy Soc A 371(1982):20120213. doi:10.1098/rsta. 2012. 0213, 2013

Lozovatsky I, Planella Morato J, Fernando HJS, Sherman K, Sanchez A (2016) Turbulence on the Carolina shelf and at the Gulf Stream Cold Wall. 48 Int Liege Coll "Submesoscale processes: mechanisms, implications and new frontiers" Liege, Belgium, May 23–27, 2016 http://gher-diva.phys.ulg.ac.be/PresentationManager/ILC2016/presentations/ILC2016-116.pdf

Lueck R, Osborn T (1984) The dissipation of kinetic energy in a warm-core ring. J Geophys Res 91(C1):803–818

MacKinnon JA, Gregg MC (2003) Mixing on the late-summer New England Shelf—solibores, shear, and stratification. J Phys Oceanogr 33:1476–1492

McWilliams JC (1985) Submesoscale, coherent vortices in the ocean. Rev Geophys 23:165–182

McWilliams JC (2008) Fluid dynamics at the margin of rotational control. Environ Fluid Mech 8:441–449

Nasmyth PW (1970) Oceanic turbulence. Ph. D. Dissertation, University of British Columbia, Vancouver.

Oakey S, Elliott JA (1977) Vertical temperature gradient structure across the Gulf Stream. J Geophys Res 82:1369–1380

Osborn TR (1980) Estimates of the local rate of vertical diffusion from dissipation measurements. J Phys Oceanogr 10(1):83–89

Pollard RT, Rhines PB, Thompson RORY (1972) The deepening of the wind-mixed layer. Geophys Fluid Dyn 4(1):381–404

Panchev S, Kesich D (1969) Energy spectrum of isotropic turbulence at large wavenumbers. Comptes Rendus de l'Academie Bulgare des Sciences 22:627–630

Rennie SE, Largier J, Lentz SJ (1999) Observations of a pulsed buoyancy current downstream of Chesapeake Bay. J Geophys Res 104(C8): 18, 227–18, 240

Roget E, Lozovatsky I, Sanchez X, Figueroa M (2006) Microstructure measurements in natural waters: methodology and applications. Prog Oceanogr 70:123–148

Ruddick B (1983) A practical indicator of the stability of the water column to double-diffusive activity. Deep-Sea Res 30(lOA):1105–1107

Shay TJ, Gregg MC (1986) Convectively driven turbulent mixing in the upper ocean. J Phys Oceanogr 16:1777–1798

Shcherbina AY, Sundermeyer MA, Kunze E, D'Asaro E et al (2015) The LATMIX summer campaign. Submesoscale stirring in the upper ocean. BAMS 96:1257–1279

St. Laurent L (2009) Turbulence and prey field properties of Gulf Stream frontal eddies on the shelf break. http://www.whoi.edu/page/preview.do?pid=96770&tid=3622&cid=59776)

St. Laurent L, Simmons H, Tang TY, Wang YH (2011) Turbulent properties of internal waves in the South China Sea. Oceanography 24(4):78–87

Strang EJ, Fernando HJS (2001) Entrainment and mixing in stratified shear flows. J Fluid Mech 428:349–386

Thomas L, Tandon A, Mahadevan A (2008) Submesoscale processes and dynamics. Ocean modeling in an eddying regime. Geophys Monograph Series 177:17–38. doi:10.1029/177GM04

Thomas LN, Taylor JR, D'Asaro EA, Lee CM, Klymak JM, Shcherbina A (2016) Symmetric instability, inertial oscillations, and turbulence at the Gulf Stream front. J Phys Oceanogr 46:197–217

Thompson WT, Haack T (2011) An investigation of sea surface temperature influence on microwave refractivity: the Wallops-2000 experiment. J Appl Meteorol Climatol 50:2319–2337

Turner JS (1973) Buoyancy effects in fluids, vol 367. Cambridge Univ Press, Cambridge

Winkel DP, Gregg MC, Sanford TB (2002) Patterns of shear and turbulence across the Florida current. J Phys Oceanogr 32:3269–3285

Wijesekera H, Shroyer E, Tandon A, Ravichandran M et al (2016) ASIRI. An ocean–atmosphere initiative for Bay of Bengal. BAMS 97: 1859–1884